

# Yang monopoles and emergent three-dimensional topological defects in interacting bosons

Yangqian Yan, Qi Zhou

*Department of Physics and Astronomy, Purdue University, West Lafayette, IN, 47906*

(Dated: February 25, 2022)

Yang monopole as a zero-dimensional topological defect has been well established in multiple fields in physics. However, it remains an intriguing question to understand interaction effects on Yang monopoles. Here, we show that collective motions of many interacting bosons give rise to exotic topological defects that are distinct from Yang monopoles seen by a single particle. Whereas interactions may distribute Yang monopoles in the parameter space or glue them to a single giant one of multiple charges, three-dimensional topological defects also arise from continuous manifolds of degenerate many-body eigenstates. Their projections in lower dimensions lead to knotted nodal lines and nodal rings. Our results suggest that ultracold bosonic atoms can be used to create emergent topological defects and directly measure topological invariants that are not easy to access in solids.

Yang monopoles play a crucial role in non-abelian gauge theories and have influential impacts in multiple subareas of physics [1]. In high energy physics, they lay the foundation of Yang-Mills theory and standard model [2–6]. In condensed matter physics, they give rise to nontrivial topological quantum states characterized by the second Chern number,  $C_2$  [7–9]. In a 5D parameter space, a Yang monopole represents a zero-dimensional point defect with a four-fold degeneracy. Away from a Yang monopole, a spin-3/2 or pseudospin-3/2 could see such point topological defect from either local non-abelian Berry curvatures or  $C_2$ . When a 4D surface encloses the Yang monopole,  $C_2 = 1$ . One could view a Yang monopole as a magnetic monopole of “charge” 1.

Whereas Yang monopoles remained a theoretical concept for decades, Sugawa, *et al.*, at NIST delivered a Yang monopole for the first time in laboratories by engineering the couplings among four hyperfine spin states of ultracold bosonic atoms [10]. Each boson in this experiment represents a pseudospin-3/2. While many experiments have used bosons to probe local abelian Berry curvatures [11–13],  $C_2$  has been extracted in the NIST experiment by integrating the non-abelian Berry curvature on 4D surfaces. Very recently,  $C_2$  has also been measured in optical lattices and photonic crystals [14, 15].

Though Yang monopoles have been well established in non-interacting systems, a fundamental question remains. Are topological defects seen by a collection of many interacting spin-3/2s the same as those seen by each individual one? In this Letter, we show that interactions allow physicists to access completely different topological defects arising from collective motions of many particles. These emergent topological defects signify the vital importance of interactions on Yang monopoles, and demonstrate the power of ultracold atoms in creating and detecting novel topological phenomena that are not easy to access in solids.

Our main results are summarized as follows. For odd particle numbers  $N$ , repulsive interactions distribute

Yang monopoles on a quantization axis in the parameter space, and attractive interactions glue them to a single one of “charge”  $N^2$  at the origin. In contrast, for  $N = 4n + 2$ , where  $n$  is a non-negative integer, interactions produce multiple 3D topological defects. When  $N = 4n$ , the many-body ground state is unique for repulsive interactions, and no topological defect can be seen by the ground state. The results of attractive interactions are similar to those for  $N = 4n + 2$ . Here, 3D defects emerge purely from interaction effects in bosons, unlike those studied in non-interacting electronic systems [16–20]. We also show how to use ultracold bosons to directly measure the topological invariants in laboratories.

Our work was motivated by a recent paper by Ho and Li [21]. Based on a mean field approach, this pioneering work shows that a Yang monopole may be stretched into an extended manifold due to interactions. In this mean field approach, all pseudospin-3/2s are described by the same condensate wave function. Here, we provide an exact solution for a generic  $N$  pseudospin-3/2 system. We show that the many-body ground state becomes degenerate in certain locations in the parameter space. These degenerate many-body eigenstates give rise to novel topological defects beyond mean field predictions.

*Hamiltonian.* The single-particle Hamiltonian that describes a Yang monopole reads [20, 21]

$$\hat{K} = -R_z \tau_z \otimes \hat{n} \cdot \vec{\sigma} - R_x \tau_x - R_y \tau_y, \quad (1)$$

where  $\vec{\sigma}$  and  $\vec{\tau}$  are two spin-1/2 operators, and  $\hat{n}$  is a unit vector. A single-mode approximation has been taken for the orbital part of the wavefunction, i.e., bosons share the same spatial wavefunction. Eq.(1) defined in a 5D parameter space,  $\mathbf{R} = (R_x, R_y, R_z n_x, R_z n_y, R_z n_z)$ , describes a spin-3/2 particle. In the NIST experiment, the first (second) two parameters are determined by the intensities and phases of radio-frequency (micro-wave) coupling and the last one,  $R_z n_z$ , is adjusted by the detuning [10]. For convenience of later discussions, We rewrite

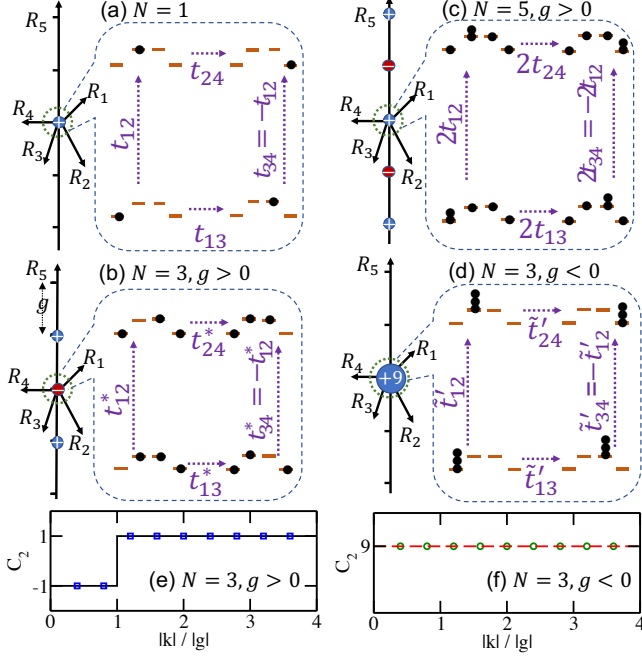


FIG. 1. Yang monopoles for odd  $N$ . Blue (red) spheres show the positively (negatively) charged monopoles with charges denoted. (a-c),  $g > 0$ ,  $N = 1, 3, 5$ . (d)  $g < 0$ ,  $N = 3$ . Insets illustrate effective Hamiltonians near the origin. Orange solid lines (black dots) represent single particle states (bosons). Dotted arrows show effective couplings. (e-f)  $C_2$  as a function of the radius  $|k|$  of the 5D sphere for three particles. Solid and dashed lines (squares and circles) are analytical (numerical) results.

this Hamiltonian,

$$\hat{K} = \sum_{i=1}^4 \epsilon_i \hat{a}_i^\dagger \hat{a}_i + \sum_{j=2}^4 \sum_{i=1}^{j-1} (t_{ij} \hat{a}_i^\dagger \hat{a}_j + h.c.), \quad (2)$$

which describes four lattice sites coupled by certain inter-site tunnelings  $t_{ij}$ , as shown in Fig. 1(a).  $\hat{a}_i^\dagger$  ( $\hat{a}_i$ ) is the creation (annihilation) operator at site  $i$ .  $\epsilon_i$  is the onsite energy,  $-\epsilon_1 = \epsilon_2 = \epsilon_3 = -\epsilon_4 = R_z n_z$ ,  $t_{13} = t_{24} = -R_x + iR_y$ ,  $t_{12} = -t_{34} = -R_z n_x + iR_z n_y$ , and  $t_{14} = t_{23} = 0$ . The 5D parameter space is now spanned by the complex tunnelings  $t_{12}$  and  $t_{13}$ , and  $R_z n_z$  that determines the onsite energies. As this pseudospin-3/2 Hamiltonian respects time reversal symmetry, every eigenstate is doubly degenerate, consistent with Kramers theorem. For many-body systems, we consider the Hamiltonian,

$$\hat{H} = \hat{K} + \hat{U}, \quad \hat{U} = g \sum_{i=1}^4 (\hat{a}_i^\dagger \hat{a}_i)^2 = g \sum_{i=1}^4 n_i^2 \quad (3)$$

where  $g$  is the onsite interaction strength.  $n_i$  represents the occupation in the  $i$ th lattice site and  $\sum_{i=1}^4 n_i = N$  is satisfied. Because  $\hat{U}$  respects the time reversal symmetry, for odd  $N$ , the Kramers theorem still applies.

Though inter-spin interactions exist in the NIST experiment, here, we concretize the discussions on intra-spin interactions, which corresponds to onsite interactions in Eq.(3), to reveal fundamental interaction effects on Yang monopoles. A Yang monopole may also be realized alternatively using coupled four lattice sites described by Eq.(2) [22]. It is then natural to consider  $\hat{H}$  in Eq. (3) as onsite interactions dominate.

We solve  $\hat{H}$  exactly and obtain the many-body eigenstates  $|\Psi_m\rangle$  for  $N$  bosons.  $|\Psi_m\rangle$  is expanded using Fock states,  $|\Psi_m\rangle = \sum_{\{n_i\}} \alpha_m \{n_i\} |n_1, n_2, n_3, n_4\rangle$ . When nodal points are observed, we compute  $C_2$  [5, 6, 22],

$$C_2 = \frac{1}{32\pi^2} \int_{S^4} d\mathbf{R} \epsilon_{\mu\nu\rho\lambda} (\text{Tr}[F_{\mu\nu} F_{\rho\lambda}] - \text{Tr}[F_{\mu\nu}] \text{Tr}[F_{\rho\lambda}]), \quad (4)$$

where  $F_{\mu\nu} = \partial_\mu A_\nu - \partial_\nu A_\mu + i[A_\mu, A_\nu]$ ,  $A_\nu^{mn} = -i\langle\Psi_m|\partial_\mu|\Psi_n\rangle$ . Matrix  $F_{\mu\nu}$  and  $A_\mu$  are nonabelian Berry curvature and nonabelian Berry connection for the ground state manifold, respectively.  $S^4$  is a closed 4D surface in the parameter space and  $\epsilon_{\mu\nu\rho\lambda}$  is Levi-Civita symbol. When nodal lines or rings are observed, corresponding topological invariants are computed.

Away from the origin of the parameter space, the single-particle ground state becomes two-fold degenerate. Thus, for  $N$  non-interacting bosons, there are  $N+1$  degenerate ground states and  $C_2$  reads  $N(N+1)(N+2)/6$  [22]. Turning on interactions, results become completely different.

*N Yang monopoles.* When  $g > 0$ , there are  $N$  points on the  $R_5$  axis, where the many-body ground state becomes four-fold degenerate. At the origin,  $\hat{K} = 0$ , there are four ways to distribute  $N \in \text{odd}$  bosons in four equivalent lattice sites to minimize the interaction energy, as shown in Fig. 1(b-c). Away from the origin, four-fold degenerate points also exist on the  $R_5$  axis. All tunnelings in Eq. (2) vanish on this axis, as  $R_{i \neq 5} = 0$ . Many-body eigenstates are simply Fock states. The mismatch of onsite energies  $\epsilon_1 - \epsilon_2 = \epsilon_4 - \epsilon_3$  could exactly compensate the penalty of interaction energy for moving one boson from one lattice site to another. For example, for  $N = 3$  and  $R_5 = g$ , states  $|1, 1, 0, 1\rangle$ ,  $|1, 0, 1, 1\rangle$ ,  $|2, 0, 0, 1\rangle$ , and  $|1, 0, 0, 2\rangle$  become degenerate. For any  $N$ , the separation between two nearest points is given by  $\Delta R_5 = g$ .

Away from these four-fold degenerate points, the four Fock states are no longer degenerate, and tunnelings become finite. In the vicinity of each degenerate point, we construct an effective model using the four nearly degenerate states as the basis. Such effective model has exactly the same formula as the single-particle Hamiltonian in Eq. (2) except that  $\epsilon_i$  and  $t_{ij}$  are modified. We show, e.g., the effective Hamiltonian near the origin, in

which the parameters read

$$\tilde{\epsilon}_i = (-1)^{\frac{N-1}{2}} \epsilon_i, \tilde{t}_{ij} = \begin{cases} t_{ij}(N+3)/4 & \text{for } N=1, 5, \dots \\ t_{ij}^*(N+1)/4 & \text{for } N=3, 7, \dots \end{cases} \quad (5)$$

Thus, we conclude that each four-fold degenerate point corresponds to a Yang monopole. A subtle difference between  $N = 1, 5, \dots$  and  $N = 3, 7, \dots$  exists. As shown in Fig. 1(b-c), it is a particle and a hole that tunnels in the effective Hamiltonian for these two cases, respectively. The “charge” of the Yang monopole at the origin for  $N = 1, 5, \dots$  is 1 and that for  $N = 3, 7, \dots$  is  $-1$ . Similarly, for a fixed  $N$ , with increasing distance to the origin, the “charges” of monopoles alternate [22]. When all monopoles are enclosed,  $C_2 = 1$ .

*A giant Yang monopole.* For attractive interactions, only one monopole exists in the parameter space, and its “charge” is  $N^2$ . At the origin,  $|N, 0, 0, 0\rangle$ ,  $|0, N, 0, 0\rangle$ ,  $|0, 0, N, 0\rangle$ ,  $|0, 0, 0, N\rangle$  are the four degenerate many-body ground states, as all bosons prefer to occupy the same lattice site to minimize the interaction energy. Away from the origin, an effective model, which has the same formula as Eq. (2), can be constructed. Since a single-particle tunneling  $t_{ij}$  moves one boson from one lattice site to another, it requires  $N$  steps of single-particle tunneling to couple these states. The parameters in the effective Hamiltonian read

$$\tilde{\epsilon}'_i = N\epsilon_i \text{ and } \tilde{t}'_{ij} = c_N t_{ij}^N / g^{N-1}, \quad (6)$$

where  $c_N$  is a function of  $N$  [22]. Using this effective model, we obtain that the “charge” of the monopole is  $N^2$  [Fig. 1(d)]. The superposition of the four Fock states actually forms a Schrodinger cat state [23–26]. Though not stable for large  $N$ , in a few-body system [27, 28], a small cat could exist in laboratories such that a Yang monopole of “charge”  $N^2$  is observable.

$C_2$  for any closed surface is equal to the total “charge” of the monopoles it encloses. If a smooth deformation of the surface does not touch a Yang monopole,  $C_2$  remains unchanged. We numerically calculate  $C_2$  of 3 particles on a 4D sphere as a function of the radius of the sphere. Fig. 1(e-f) show that  $C_2$  is indeed given by the total “charge” of the monopole enclosed in the sphere. Note that  $C_2$  is much smaller than that of non-interacting systems. This is because an infinitesimal interaction reduces the  $N+1$  fold degeneracy of non-interacting systems to a two-fold one. Nevertheless, we have verified that, the total  $C_2$  of the lowest  $N+1$  bands for weakly interacting systems is indeed the same as that for the corresponding non-interacting systems.

*3D topological defects.* If the average particle number per site is an integer, i.e.,  $N = 4n$ , where  $n$  is a positive integer, the many-body ground state becomes unique for  $g > 0$ . This is best understood in the strongly interacting regime. As bosons prefer to distribute evenly in the

four lattice sites to minimize the interaction energy, the unique ground state cannot see any topological defects. When  $g < 0$ , the many-body ground state is four-fold degenerate at the origin of the parameter space, similar to the case of odd particles. Away from the origin, an effective Hamiltonian can be constructed in the same manner. However, the resultant effective Hamiltonian is distinct. The effective coupling between the Fock states, such as  $|N, 0, 0, 0\rangle$  and  $|0, N, 0, 0\rangle$ , now requires an even number steps of single-particle tunnelings. In the single-particle Hamiltonian in Eq. (2),  $t_{12}$  and  $t_{34}$  have different signs. This minus sign remains unchanged in the effective model for odd  $N$ , as both effective couplings,  $\tilde{t}'_{12}$  and  $\tilde{t}'_{34}$ , are proportional to odd powers of  $t_{12}$  and  $t_{34}$ .

For even particle numbers, the minus sign disappears. Completely different topological defects arise. The effective Hamiltonian reads

$$\hat{H}_{\text{eff}} = a\tilde{\tau}_z \otimes \tilde{\sigma}_z + b\tilde{\tau}_x \otimes I + c\tilde{\tau}_y \otimes I + dI \otimes \tilde{\sigma}_x + eI \otimes \tilde{\sigma}_y, \quad (7)$$

where  $a = -2R_5$ ,  $b = -(R_1^2 - R_2^2)/g$ ,  $c = -2R_1R_2/g$ ,  $d = -(R_3^2 - R_4^2)/g$ , and  $e = -2R_3R_4/g$  for  $N = 2$ .  $\vec{\sigma}$  and  $\vec{\tau}$  are two spin-1/2s, and  $I$  the identity matrix. The eigenstates of  $\tilde{\tau}_z \otimes \tilde{\sigma}_z$ ,  $|\uparrow\uparrow\rangle$ ,  $|\uparrow\downarrow\rangle$ ,  $|\downarrow\uparrow\rangle$ ,  $|\downarrow\downarrow\rangle$ , correspond to  $|N, 0, 0, 0\rangle$ ,  $|0, N, 0, 0\rangle$ ,  $|0, 0, N, 0\rangle$ ,  $|0, 0, 0, N\rangle$ . The eigenenergy of  $\hat{H}_{\text{eff}}$  reads

$$E = \pm \sqrt{a^2 + (\sqrt{b^2 + c^2} \pm \sqrt{d^2 + e^2})^2}, \quad (8)$$

which shows that eigenstates become degenerate in certain 3D continuous manifolds.

$\{\mathcal{M}_1: R_1 = R_2 = 0\}$  and  $\{\mathcal{M}'_1: R_3 = R_4 = 0\}$ , both the ground and excited states are doubly degenerate.

$\{\mathcal{M}_2: R_5 = 0, R_1^2 + R_2^2 = R_3^2 + R_4^2\}$ , the second and third states are degenerate, and the ground state (the fourth state) is unique.

As Kramers theorem does not apply to even number of spin-3/2s, the even-fold degeneracy is not guaranteed and  $\mathcal{M}_2$  is possible here. These three manifolds intersect at the origin of the 5D parameter space. Away from them, there is no degeneracy.  $\mathcal{M}_2$  signifies the vanishing gap between the lowest and the highest two states on any closed 4D surface. Thus,  $C_2$  is no longer appropriate to characterize the topological defects. Each manifold is characterized by its own corresponding topological invariant. Meanwhile, the projections of them in lower dimensions lead to knotted nodal lines and rings.

Since  $\mathcal{M}_1$  and  $\mathcal{M}_2$  are 3D defects in a 5D parameter space, a 1D loop can be defined without intersecting them. We calculate the Berry phase  $\gamma_m = -i \oint_M d\mathbf{R} \cdot \langle \Psi_m | \nabla_{\mathbf{R}} | \Psi_m \rangle$  for the  $m$ -th eigenstate  $|\Psi_m\rangle$ , where  $M$  denotes a closed loop in the parameter space. For any loop that does not interlock the defects, i.e., loop that can shrink to a single point without closing the gap,  $\gamma_m = 0$ . For a loop interlocking the defects, whether  $\gamma_1 + \gamma_2 = 0$  or  $\pi$  (or their multiples), defines a  $Z_2$  index  $\zeta_1$  for the

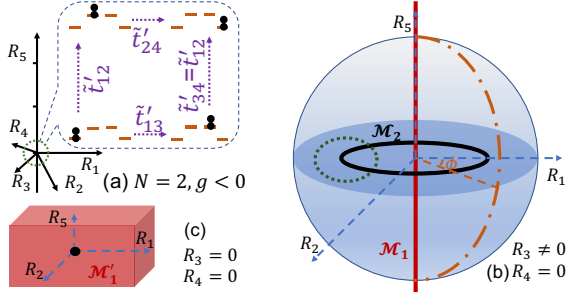


FIG. 2. (a) The effective Hamiltonian for two particles with  $g < 0$ . (b-c) shows the projections of the defects in a 3D subspace with fixed  $R_3$  and  $R_4$ . (b) The red line (black ring) shows the projection of  $\mathcal{M}_1$  ( $\mathcal{M}_2$ ). The green dotted circle (blue 2D sphere) is used to calculate  $\zeta_1$  ( $\zeta_2$ ). The dash-dotted longitude connecting the north and south poles defines a  $\phi$ -dependent Wilson line. (c) When  $\mathcal{M}_2$  reduces to a point at the origin,  $\mathcal{M}_1$  occupies the entire 3D subspace (red box).

defects [19]. For  $M_1$  and  $M'_1$ , we find that  $\gamma = N\pi$  for all eigenstates and  $\zeta_1 = 0$ . For  $M_2$ , we find that  $\gamma = (0, \pi, \pi, 0)$  for each eigenstate and  $\zeta_1 = 1$ .

To better visualize this  $Z_2$  invariant, we project  $\mathcal{M}_1$ ,  $\mathcal{M}'_1$  and  $\mathcal{M}_2$  to lower dimensions, i.e., reducing the dimension by fixing the values of certain parameters. Defining  $\vec{m} = (d, e)$  and  $|\vec{m}| = \sqrt{d^2 + e^2} = (R_3^2 + R_4^2)/|g|$ , the eigenenergies in Eq. (8) read  $E = \pm\sqrt{a^2 + (\sqrt{b^2 + c^2} \pm |\vec{m}|)^2}$ . Interestingly, this energy spectrum is identical to the one used to study nodal rings in electronic systems [19]. As shown in Fig. 2, for any finite  $|\vec{m}|$ ,  $\mathcal{M}_1$  becomes an infinite nodal line, and  $\mathcal{M}_2$  becomes a nodal ring with radius  $|\vec{m}|$ .  $\mathcal{M}'_1$  does not show up in this subspace. The dashed circles that interlock the nodal ring or line allow one to compute  $\gamma$ . Decreasing  $|\vec{m}|$ , the nodal ring shrinks and the nodal line remains unchanged. When  $|\vec{m}| = 0$ , the nodal ring reduces to a single point at the origin, and the gap does not open. In particular, this whole 3D subspace precisely becomes  $\mathcal{M}'_1$  and the eigenenergies are two-fold degenerate everywhere. For this particular set of parameters,  $\hat{H}_{\text{eff}}$  describes a quantum spin Hall effect, as  $\sigma_z = \pm 1$  corresponds to two opposite effective magnetic fields acting on  $\vec{\tau}$ . When  $\vec{m}$  changes sign, the nodal ring appears again.

On any 2D sphere that does not touch  $\mathcal{M}_2$ , the lowest two eigenstates are separated from the rest. On such sphere, the projection to the lowest  $k$  states, which are separated from the higher  $l$  states, establishes another topological invariant,  $\zeta_2$ , of the nodal ring [19, 29]. To be explicit, Wilson lines connecting the north and south pole along a half longitude depend on the polar angle  $\phi$ , as shown in Fig. (2). Such  $\phi$  dependence allows one to define a winding number  $n_w$ . For generic  $k, l > 2$ ,  $\zeta_2 = \text{mod}(n_w, 2)$  defines a  $Z_2$  index. In our system,  $k = 2$ , and the winding number becomes a  $Z$  index [19, 30]. For our effective model  $\hat{H}_{\text{eff}}$ , we find that  $\zeta_2 = 1$  for

any 2D sphere that encloses the nodal ring; Otherwise,  $\zeta_2 = 0$ . Thus, the nodal ring defines a topological phase transition where  $\zeta_2$  changes its value. For repulsive interactions,  $M_1$  and  $M'_1$  switch with  $M_2$  [22]. While the topological defects are derived in the strongly interacting regime, we numerically verified that they hold even for weakly interacting systems.

*Realizations in few-body systems.* With increasing  $N$ , the energy splitting between eigenstates decreases. Moreover, due to the small scattering length  $a_s$  and the extended orbital wavefunction in the NIST experiment, interaction strength  $g$  is very weak. For instance, for  $a_s = 5\text{nm}$ ,  $N = 10^5$ , trapping frequency  $\omega = 2\pi * 70\text{Hz}$ ,  $g \approx 0.04\text{Hz}$ , which is too weak to have significant effects. The main experimental results are well explained by non-interacting pictures. Thus, to better resolve these topological defects and the associated topological invariants, experimentalists could use few-body systems to reduce  $N$  and increase  $g$ .

A 2D optical superlattice is a promising platform to realize Hamiltonians in Eq. (3) and Eq. (7) in the real space. Such superlattice divides the system into many isolated plaquettes, each of which contains four sites. Currently available experimental techniques allow experimentalists to dress and detect each individual plaque. Many interesting few-body phenomena have been explored [31–33]. Using laser-assisted tunneling and magnetic field gradient, both the amplitude and phase of the tunnelings can be engineered [32, 34]. The onsite potential can be tuned by superposing an additional 1D lattice tilted by  $45^\circ$ . The Hamiltonian in Eq. (1) can then be delivered. Turning on interactions, the effective Hamiltonian in Eq. (7) could then be explored. For instance, the interaction strength is around 100Hz for Rb in optical lattices with laser wavelength of 767nm and depth of  $8E_R$ , where  $E_R$  is the characteristic energy scale defined by the wavelength. Increasing the lattice depth or the scattering length,  $g$  can be further enhanced. Using realistic experimental parameters, we find that the previously discussed topological defects can indeed be resolved [22]. Experimentalists can also realize Eq. (7) directly in non-interacting systems by engineering the inter-site couplings. A few other approaches, including mesoscopic traps, optical tweezers, ion traps and superconducting circuits, can also be used to study few-body physics related to our work [22, 27, 28].

A unique advantage of ultracold atoms is that topological defects and the associated topological invariants can be directly probed. To measure  $\zeta_1$ , the local Berry curvature could be measured to extract the Berry phase accumulated in a 1D loop [10, 11, 35–39]. To measure  $\zeta_2$ , Wilson lines can be measured in the same manner in Ref. [40].

In the NIST experiment on spinor BEC, inter-spin interactions exist. Thus, we need to consider generic interactions  $\sum_i g_i n_i^2 + \sum_{i < j} g_{ij} n_i n_j$ , where  $g_i$  ( $g_{ij}$ ) is the



intra (inter) spin interaction strength. If such interactions preserve time reversal symmetry, our main results remain unchanged. For interactions that break time reversal symmetry, even richer physics regarding topological defects arises [22].

In conclusion, we have shown that interactions give rise to emergent topological defects distinct from those seen by each individual particle. Depending on the total particle number and interaction strength, either giant Yang monopoles of multiple charges or 3D continuous topological defects emerge. Such topological defects can be accessed in current experiments, in particular, those on few-body systems. While Dirac monopoles control many 2D and 3D topological matters, Yang monopoles and  $C_2$  are crucial for topological quantum phenomena in high dimensions, including 4D quantum Hall effects. Nodal lines and nodal rings as continuous topological defects also provide physicists unprecedented topological quantum matters. We hope that our work will stimulate more studies on using ultracold atoms to create and measure topological defects in high dimensional interacting systems.

QZ acknowledges useful discussions with T.L. Ho, I. Spielman, S. Sugawa, and C. Fang. YY acknowledges useful discussions with C. Li. This work is supported by startup funds from Purdue University.

- 
- [1] C. N. Yang and R. L. Mills, "Conservation of Isotopic Spin and Isotopic Gauge Invariance," *Phys. Rev.* **96**, 191 (1954).
  - [2] C. N. Yang, "Generalization of Diracs monopole to  $SU_2$  gauge fields," *J. Math. Phys.* **19**, 320 (1978).
  - [3] G. 't Hooft, "The standard model of particle physics," *Nature (London)* **448**, 270 (2007).
  - [4] G. 't Hooft, "Magnetic monopoles in unified gauge theories," *Nucl. Phys. B* **79**, 276 (1974).
  - [5] S.-S. Chern, "Characteristic Classes of Hermitian Manifolds," *Ann. Math.* **47**, 85 (1946).
  - [6] S. Chern, *Topics in differential geometry* (The Institute for Advanced Study, Princeton, 1951).
  - [7] C.-H. Chern, H.-D. Chen, C. Wu, J.-P. Hu, and S.-C. Zhang, "Non-Abelian Berry phase and Chern numbers in higher spin-pairing condensates," *Phys. Rev. B* **69**, 214512 (2004).
  - [8] D. Xiao, J. Shi, D. P. Clougherty, and Q. Niu, "Theory of electric polarization induced by inhomogeneity in crystals," (2007), [arXiv:0711.1855](https://arxiv.org/abs/0711.1855).
  - [9] X.-L. Qi, T. L. Hughes, and S.-C. Zhang, "Topological field theory of time-reversal invariant insulators," *Phys. Rev. B* **78**, 195424 (2008).
  - [10] S. Sugawa, F. Salces-Carcoba, A. R. Perry, Y. Yue, and I. B. Spielman, "Observation of a non-Abelian Yang Monopole: From New Chern Numbers to a Topological Transition," [arXiv:1610.06228](https://arxiv.org/abs/1610.06228).
  - [11] M. Atala, M. Aidelsburger, J. T. Barreiro, D. Abanin, T. Kitagawa, E. Demler, and I. Bloch, "Direct measurement of the Zak phase in topological Bloch bands," *Nat. Phys.* **9**, 795 (2013).
  - [12] M. Aidelsburger, M. Lohse, C. Schweizer, M. Atala, J. T. Barreiro, S. Nascimbène, N. R. Cooper, I. Bloch, and N. Goldman, "Measuring the Chern number of Hofstadter bands with ultracold bosonic atoms," *Nat. Phys.* **11**, 162 (2015).
  - [13] M. Lohse, C. Schweizer, O. Zilberberg, M. Aidelsburger, and I. Bloch, "A Thouless quantum pump with ultracold bosonic atoms in an optical superlattice," *Nat. Phys.* **12**, 350 (2016).
  - [14] M. Lohse, C. Schweizer, H. M. Price, O. Zilberberg, and I. Bloch, "Exploring 4D Quantum Hall Physics with a 2D Topological Charge Pump," *Nature (London)* **553**, 55 (2018).
  - [15] O. Zilberberg, S. Huang, J. Guglielmon, M. Wang, K. Chen, Y. E. Kraus, and M. C. Rechtsman, "Photonic topological boundary pumping as a probe of 4D quantum Hall system," *Nature (London)* **553**, 59 (2018).
  - [16] A. A. Burkov, M. D. Hook, and L. Balents, "Topological nodal semimetals," *Phys. Rev. B* **84**, 235126 (2011).
  - [17] A. P. Schnyder, P. M. R. Brydon, and C. Timm, "Types of topological surface states in nodal noncentrosymmetric superconductors," *Phys. Rev. B* **85**, 024522 (2012).
  - [18] P. Hosur, X. Dai, Z. Fang, and X.-L. Qi, "Time-reversal-invariant topological superconductivity in doped Weyl semimetals," *Phys. Rev. B* **90**, 045130 (2014).
  - [19] C. Fang, Y. Chen, H.-Y. Kee, and L. Fu, "Topological nodal line semimetals with and without spin-orbital coupling," *Phys. Rev. B* **92**, 081201 (2015).
  - [20] B. Lian and S.-C. Zhang, "Five-dimensional generalization of the topological Weyl semimetal," *Phys. Rev. B* **94**, 041105 (2016).
  - [21] T.-L. Ho and C. Li, "The Chern Numbers of Interaction-stretched Monopoles in Spinor Bose Condensates," [arXiv:1704.03833](https://arxiv.org/abs/1704.03833).
  - [22] See the supplemental materials at TO-BE-INSERT-BY-THE-EDITOR, which includes Ref. [41–45], for detailed derivations of non-interacting  $C_2$ , location and charge of the Yang monopole for odd  $N$  and positive  $g$ ,  $C_2$  for odd  $N$ , expression for  $c_N$ , topological invariants, 3D topological defects for even number of particles with repulsive interaction, linking number, experimental schemes for explore few-body physics, and generic interaction.
  - [23] W. H. Zurek, "Decoherence and the transition from quantum to classical," *Phys. Today* **44**, 36 (1991).
  - [24] C. Monroe, D. M. Meekhof, B. E. King, and D. J. Wineland, "A "Schrodinger Cat" Superposition State of an Atom," *Science* **272**, 1131 (1996).
  - [25] T.-L. Ho and C. V. Ciobanu, "The Schrödinger Cat Family in Attractive Bose Gases," *J. Low Temp. Phys.* **135**, 257 (2004).
  - [26] E. J. Mueller, T.-L. Ho, M. Ueda, and G. Baym, "Fragmentation of Bose-Einstein condensates," *Phys. Rev. A* **74**, 033612 (2006).
  - [27] A. N. Wenz, G. Zürn, S. Murmann, I. Brouzos, T. Lompe, and S. Jochim, "From Few to Many: Observing the Formation of a Fermi Sea One Atom at a Time," *Science* **342**, 457 (2013).
  - [28] G. Zürn, A. N. Wenz, S. Murmann, A. Bergschneider, T. Lompe, and S. Jochim, "Pairing in Few-Fermion Systems with Attractive Interactions," *Phys. Rev. Lett.* **111**, 175302 (2013).
  - [29] A. Hatcher, *Algebraic Topology* (Cambridge University Press, Cambridge, UK, 2002).

- [30] Chen Fang and Hongming Weng and Xi Dai and Zhong Fang, “Topological nodal line semimetals,” *Chin. Phys. B* **25**, 117106 (2016).
- [31] S. Nascimbène, Y.-A. Chen, M. Atala, M. Aidelsburger, S. Trotzky, B. Paredes, and I. Bloch, “Experimental Realization of Plaquette Resonating Valence-Bond States with Ultracold Atoms in Optical Superlattices,” *Phys. Rev. Lett.* **108**, 205301 (2012).
- [32] M. Aidelsburger, M. Atala, M. Lohse, J. T. Barreiro, B. Paredes, and I. Bloch, “Realization of the hofstadter hamiltonian with ultracold atoms in optical lattices,” *Phys. Rev. Lett.* **111**, 185301 (2013).
- [33] H.-N. Dai, B. Yang, A. Reingruber, H. Sun, X.-F. Xu, Y.-A. Chen, Z.-S. Yuan, and J.-W. Pan, “Four-body ring-exchange interactions and anyonic statistics within a minimal toric-code Hamiltonian,” *Nat. Phys.* **13**, 1195 (2017).
- [34] H. Miyake, G. A. Siviloglou, C. J. Kennedy, W. C. Burton, and W. Ketterle, “Realizing the Harper Hamiltonian with Laser-Assisted Tunneling in Optical Lattices,” *Phys. Rev. Lett.* **111**, 185302 (2013).
- [35] V. Gritsev and A. Polkovnikov, “Dynamical quantum hall effect in the parameter space,” *Proc. Natl. Acad. Sci.* **109**, 6457 (2012).
- [36] H. M. Price and N. R. Cooper, “Mapping the Berry curvature from semiclassical dynamics in optical lattices,” *Phys. Rev. A* **85**, 033620 (2012).
- [37] P. Hauke, M. Lewenstein, and A. Eckardt, “Tomography of Band Insulators from Quench Dynamics,” *Phys. Rev. Lett.* **113**, 045303 (2014).
- [38] L. Duca, T. Li, M. Reitter, I. Bloch, M. Schleier-Smith, and U. Schneider, “An Aharonov-Bohm interferometer for determining Bloch band topology,” *Science* **347**, 288.
- [39] M. Kolodrubetz, “Measuring the Second Chern Number from Nonadiabatic Effects,” *Phys. Rev. Lett.* **117**, 015301 (2016).
- [40] T. Li, L. Duca, M. Reitter, F. Grusdt, E. Demler, M. Endres, M. Schleier-Smith, I. Bloch, and U. Schneider, “Bloch state tomography using Wilson lines,” *Science* **352**, 1094 (2016).
- [41] G. Jotzu, M. Messer, R. Desbuquois, M. Lebrat, T. Uehlinger, D. Greif, and T. Esslinger, “Experimental realization of the topological Haldane model with ultracold fermions,” *Nature (London)* **515**, 237 (2014).
- [42] C. V. Parker, L.-C. Ha, and C. Chin, “Direct observation of effective ferromagnetic domains of cold atoms in a shaken optical lattice,” *Nat. Phys.* **9**, 769 (2013).
- [43] A. Kaufman, B. Lester, M. Foss-Feig, M. Wall, A. Rey, and C. Regal, “Entangling two transportable neutral atoms via local spin exchange,” *Nature (London)* **527**, 208 (2015).
- [44] P. Roushan, C. Neill, Y. Chen, M. Kolodrubetz, C. Quintana, N. Leung, M. Fang, R. Barends, B. Campbell, Z. Chen, *et al.*, “Observation of topological transitions in interacting quantum circuits,” *Nature (London)* **515**, 241 (2014).
- [45] M. D. Schroer, M. H. Kolodrubetz, W. F. Kindel, M. Sandberg, J. Gao, M. R. Vissers, D. P. Pappas, A. Polkovnikov, and K. W. Lehnert, “Measuring a Topological Transition in an Artificial Spin-1/2 System,” *Phys. Rev. Lett.* **113**, 050402 (2014).

## Supplemental Material of “Yang monopoles and emergent three-dimensional topological defects in interacting bosons”

### DEFINITION OF $C_2$

The non-abelian Berry connection  $A_\nu^{mn}$ , non-abelian Berry curvature  $F_{\mu\nu}^{mn}$ , and non-abelian second Chern number are defined as [21].

$$A_\nu^{mn} = -i\langle\Psi_m|\partial_\nu|\Psi_n\rangle, \quad F_{\mu\nu}^{mn} = \partial_\mu A_\nu^{mn} - \partial_\nu A_\mu^{mn} + i[A_\mu, A_\nu]^{mn} \quad (\text{S9})$$

$$C_2 = \frac{1}{32\pi^2} \int_{S^4} d\mathbf{R} \epsilon_{\mu\nu\rho\lambda} (\text{Tr}[F_{\mu\nu} F_{\rho\lambda}] - \text{Tr}[F_{\mu\nu}] \text{Tr}[F_{\rho\lambda}]). \quad (\text{S10})$$

### NON-INTERACTING $C_2$

Single-particle ground state of the Hamiltonian in Eq. (1) of the main text is doubly degenerate. Denote the two states as  $\psi_a$  and  $\psi_b$ , and define  $A_{\mu\nu}^{mn} = -i\langle\psi_m|\partial_\nu\psi_n\rangle$ , the Berry curvature reads

$$F_{\mu\nu}^{mn} = A_{\mu\nu}^{mn} - A_{\nu\mu}^{mn} + i[A_\mu, A_\nu]. \quad (\text{S11})$$

Because of the time-reversal symmetry, the traces of the Berry connection and the Berry curvature are zero,

$$A_\mu^{aa} = -A_\mu^{bb}, \quad \text{Tr} F_{\mu\nu} = 0. \quad (\text{S12})$$

We also have  $A_{\mu\nu}^{aa} = A_{\nu\mu}^{bb}$ . Defining

$$\tilde{A}_{\mu\nu} = \begin{pmatrix} A_{\mu\nu}^{aa} & A_{\mu\nu}^{ab} \\ A_{\mu\nu}^{ba} & -A_{\mu\nu}^{aa} \end{pmatrix} \quad (\text{S13})$$

$$\tilde{F}_{\mu\nu} = \tilde{A}_{\mu\nu} + iA_{\mu}A_{\nu}, \quad (\text{S14})$$

and using the property of the Levi-Civita symbol, we express the second Chern number using an alternative form,

$$C_2^0(1) = \frac{1}{32\pi^2} \int_{S^4} d\mathbf{R} \epsilon_{\mu\nu\rho\lambda} \text{Tr}[F_{\mu\nu}F_{\rho\lambda}] = \frac{1}{8\pi^2} \int_{S^4} d\mathbf{R} \epsilon_{\mu\nu\rho\lambda} \text{Tr}[\tilde{F}_{\mu\nu}\tilde{F}_{\rho\lambda}]. \quad (\text{S15})$$

The above results can be generalized to  $N$  particles.

For  $N$  non-interacting bosons, there are  $N + 1$  degenerate ground states. Using Fock states as basis states, the ground state reads  $|N - i, i\rangle$ , where  $i$  takes the values of  $0, 1, 2, \dots, N$ ; here  $|N - i, i\rangle$  represent the  $N - i$  bosons in state  $\psi_a$  and  $i$  bosons in state  $\psi_b$ . The Berry connection  $A_{\mu}$  and matrix  $A_{\mu\nu}$  are tridiagonal in the Fock state basis.

$$A_{\mu}^{i-1,i} = -i \langle N - i + 1, i - 1 | \partial_{\mu} | N - i, i \rangle = \sqrt{i(N - 1 + 1)} A_{\mu}^{ab} \quad (\text{S16})$$

$$A_{\mu}^{i,i-1} = -i \langle N - i, i | \partial_{\mu} | N - i + 1, i - 1 \rangle = \sqrt{i(N - 1 + 1)} A_{\mu}^{ba} \quad (\text{S17})$$

$$A_{\mu}^{i,i} = -i \langle N - i, i | \partial_{\mu} | N - i, i \rangle = (N - i) A_{\mu}^{aa} + i A_{\mu}^{bb} = (N - 2i) A_{\mu}^{aa}. \quad (\text{S18})$$

The same holds for the  $\tilde{A}_{\mu\nu}$  matrix,

$$\tilde{A}_{\mu\nu}^{i-1,i} = -i \langle N - i + 1, i - 1 | \overleftrightarrow{\partial_{\mu}} \overleftrightarrow{\partial_{\nu}} | N - i, i \rangle = \sqrt{i(N - 1 + 1)} A_{\mu\nu}^{ab} \quad (\text{S19})$$

$$\tilde{A}_{\mu\nu}^{i,i-1} = -i \langle N - i, i | \overleftrightarrow{\partial_{\mu}} \overleftrightarrow{\partial_{\nu}} | N - i + 1, i - 1 \rangle = \sqrt{i(N - 1 + 1)} A_{\mu\nu}^{ba} \quad (\text{S20})$$

$$\tilde{A}_{\mu\nu}^{i,i} = (N - 2i) A_{\mu\nu}^{aa}. \quad (\text{S21})$$

Note that  $A_{\mu}^{xy}$  and  $A_{\mu\nu}^{xy}$  are for single particle if  $x, y$  is  $a$  or  $b$  and are for  $N$  particles otherwise. Same as that for  $N = 1$ , the second Chern number for arbitrary  $N$  can also be calculated using Eq. (S5).

We break the integrand  $\epsilon_{\mu\nu\rho\lambda} \text{Tr}[\tilde{F}_{\mu\nu}\tilde{F}_{\rho\lambda}]$  into two parts,  $\epsilon_{\mu\nu\rho\lambda} \text{Tr}[\tilde{F}_{\mu\nu}\tilde{A}_{\rho\lambda}]$  and  $2i\epsilon_{\mu\nu\rho\lambda} \text{Tr}[\tilde{A}_{\mu\nu}A_{\rho}A_{\lambda}]$  (note that  $\epsilon_{\mu\nu\rho\lambda} \text{Tr}[A_{\mu}A_{\nu}A_{\rho}A_{\lambda}]$  is 0). Writing down the trace explicitly and expressing the two terms in terms of the single particle quantities, we obtain

$$\text{Tr}[\tilde{A}_{\mu\nu}\tilde{A}_{\rho\lambda}] = \sum_i \tilde{A}_{\mu\nu}^{ii} \tilde{A}_{\rho\lambda}^{ii} + \sum_i \tilde{A}_{\mu\nu}^{i,i+1} \tilde{A}_{\rho\lambda}^{i+1,i} + \sum_i \tilde{A}_{\mu\nu}^{i,i-1} \tilde{A}_{\rho\lambda}^{i-1,i} \quad (\text{S22})$$

$$= \sum_{i=0}^N (N - 2i)^2 \tilde{A}_{\mu\nu}^{aa} \tilde{A}_{\rho\lambda}^{aa} + \sum_{i=0}^{N-1} (i + 1)(N - i) \left( \tilde{A}_{\mu\nu}^{ab} \tilde{A}_{\rho\lambda}^{ba} + \tilde{A}_{\mu\nu}^{ba} \tilde{A}_{\rho\lambda}^{ab} \right) \quad (\text{S23})$$

$$\text{Tr}[\tilde{A}_{\mu\nu}A_{\rho}A_{\lambda}] = \sum_i \tilde{A}_{\mu\nu}^{ii} \left( A_{\rho}^{i,i+1} A_{\lambda}^{i+1,i} + A_{\rho}^{i,i-1} A_{\lambda}^{i-1,i} \right) \quad (\text{S24})$$

$$+ \sum_i \tilde{A}_{\mu\nu}^{i,i-1} \left( A_{\rho}^{i-1,i-1} A_{\lambda}^{i-1,i} + A_{\rho}^{i-1,i} A_{\lambda}^{i,i} \right) \quad (\text{S25})$$

$$+ \sum_i \tilde{A}_{\mu\nu}^{i,i+1} \left( A_{\rho}^{i+1,i+1} A_{\lambda}^{i+1,i} + A_{\rho}^{i+1,i} A_{\lambda}^{i,i} \right) \quad (\text{S26})$$

$$= \sum_{i=0}^N (N - 2i)(N - i)(i + 1) \left( A_{\mu\nu}^{aa} A_{\rho}^{ab} A_{\lambda}^{ba} + A_{\mu\nu}^{ba} A_{\rho}^{aa} A_{\lambda}^{ab} + A_{\mu\nu}^{ab} A_{\rho}^{ba} A_{\lambda}^{aa} \right) \quad (\text{S27})$$

$$+ \sum_{i=0}^N (N - 2i)(N - i + 1)i \left( A_{\mu\nu}^{aa} A_{\rho}^{ba} A_{\lambda}^{ab} + A_{\mu\nu}^{ba} A_{\rho}^{ab} A_{\lambda}^{aa} + A_{\mu\nu}^{ab} A_{\rho}^{aa} A_{\lambda}^{ba} \right) \quad (\text{S28})$$

Using the identity

$$\frac{1}{6} N(N + 1)(N + 2) = - \sum_{i=0}^N (N - 2i)(N - i + 1)i, \quad (\text{S29})$$

we write  $C_2^0(N)$  using  $C_2^0(1)$ ,

$$C_2^0(N) = \frac{1}{6} N(N + 1)(N + 2) C_2^0(1) = \frac{1}{6} N(N + 1)(N + 2). \quad (\text{S30})$$

## LOCATION AND CHARGE OF YANG MONOPOLES FOR ODD $N$ AND POSITIVE $g$

Along the  $R_5$  axis, all off-diagonal couplings disappear and Fock states become the eigenstates. Varying  $R_5$ , we find  $N$  possible points on this axis where there exist four-fold degeneracy.

**(a)  $N = 4m + 1$  for integer  $m$**

The four states,  $|m - l + 1, m + l, m + l, m - l\rangle$ ,  $|m - l, m + l + 1, m + l, m - l\rangle$ ,  $|m - l, m + l, m + l + 1, m - l\rangle$ , and  $|m - l, m + l, m + l, m - l + 1\rangle$  are degenerate when  $R_5 = -2lg$ , where  $l = -m, -m + 1, \dots, m - 1, m$ . The effective Hamiltonian reads

$$\tilde{\epsilon}_i = \epsilon_i \quad (\text{S31})$$

$$\tilde{t}_{ij} = t_{ij} \sqrt{(m - l + 1)(m + l + 1)}. \quad (\text{S32})$$

The extra Bose enhancement factor comparing to the single particle Hamiltonian does not change the second Chern number, so  $C_2 = 1$ .

At  $R_5 = -(2l + 1)g$ , the other four states,  $|m - l - 1, m + l + 1, m + l + 1, m - l\rangle$ ,  $|m - l, m + l, m + l + 1, m - l\rangle$ ,  $|m - l, m + l + 1, m + l, m - l\rangle$ , and  $|m - l - 1, m + l + 1, m + l + 1, m - l\rangle$  are degenerate, where  $l = -m, -m + 1, \dots, m - 2, m - 1$ . The effective Hamiltonian reads

$$\tilde{\epsilon}_i = -\epsilon_i \quad (\text{S33})$$

$$\tilde{t}_{ij} = t_{ij}^* \sqrt{(m - l)(m + l + 1)}. \quad (\text{S34})$$

The extra Bose enhancement factor together with an additional phase factor  $e^{i\pi}$  comparing to the single particle Hamiltonian does not change the second Chern number but flipping the sign of the diagonal terms changes  $C_2$  to  $-1$ .

**(b)  $N = 4m + 3$  for integer  $m$**

At  $R_5 = -2lg$ , the four states,  $|m - l, m + l + 1, m + l + 1, m - l + 1\rangle$ ,  $|m - l + 1, m + l, m + l + 1, m - l + 1\rangle$ ,  $|m - 1, m + l + 1, m + l, m - l + 1\rangle$ , and  $|m - l + 1, m + l + 1, m + l + 1, m - l\rangle$  are degenerate, where  $l = -m, -m + 1, \dots, m - 1, m$ . The effective Hamiltonian reads

$$\tilde{\epsilon}_i = -\epsilon_i \quad (\text{S35})$$

$$\tilde{t}_{ij} = t_{ij}^* \sqrt{(m - l + 1)(m + l + 1)}. \quad (\text{S36})$$

Similar to case (a),  $C_2 = -1$ .

At  $R_5 = -(2l + 1)g$ , the four states,  $|m - l + 1, m + l + 1, m + l + 1, m - l\rangle$ ,  $|m - l, m + l + 2, m + l + 1, m - l\rangle$ ,  $|m - l, m + l + 1, m + l + 2, m - l\rangle$ , and  $|m - l, m + l + 1, m + l + 1, m - l + 1\rangle$  are degenerate, where  $l = -m - 1, -m, \dots, m - 1, m$ . The effective Hamiltonian reads

$$\tilde{\epsilon}_i = \epsilon_i \quad (\text{S37})$$

$$\tilde{t}_{ij} = t_{ij} \sqrt{(m - l + 1)(m + l + 2)}. \quad (\text{S38})$$

Similar to case (a),  $C_2 = 1$ .

For example, Fig. S3(d) illustrates the effective Hamiltonian for  $N = 3$  and  $R_5 = g$ . The onsite energy different balances off the repulsive energy for the sites with two particles. Thus, all the four states has the same energy and as the coupling  $R_1, R_2, R_3, R_4$  approaches zero, the four states becomes the eigenstates and four-fold degeneracy emerges.

## EXPRESSION FOR $c_N$

At the origin,  $|N, 0, 0, 0\rangle$ ,  $|0, N, 0, 0\rangle$ ,  $|0, 0, N, 0\rangle$ ,  $|0, 0, 0, N\rangle$  are the four degenerate many-body ground states. Treating the  $|R|$  as a small parameter, the lowest order coupling reads

$$\langle N, 0, 0, 0 | \hat{H}_{\text{eff}} | 0, N, 0, 0 \rangle = \frac{\prod_{i=0}^{N-1} \langle N - i, i, 0, 0 | \hat{K} | N - i - 1, i + 1, 0, 0 \rangle}{\prod_{i=1}^{N-1} \left( \langle N - i, i, 0, 0 | \hat{U} | N - i, i, 0, 0 \rangle - \langle N, 0, 0, 0 | \hat{U} | N, 0, 0, 0 \rangle \right)}. \quad (\text{S39})$$



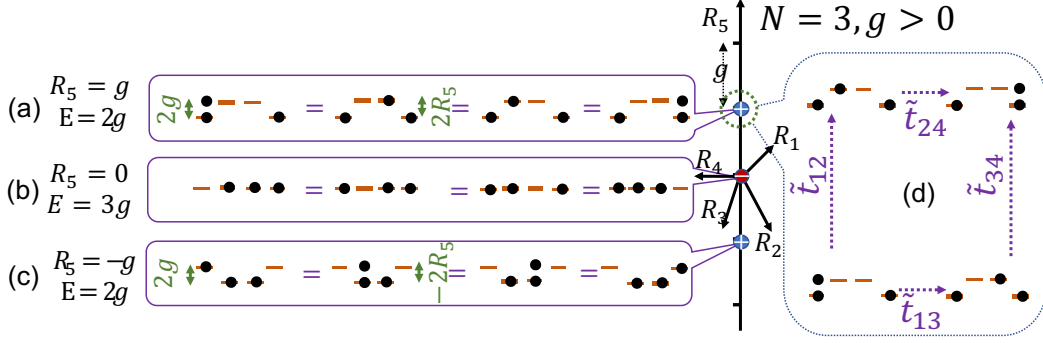


FIG. S3. (Color online) Schematic of Yang monopoles for 3 particles with positive interaction strength  $g$ . Blue (red) spheres show the positively (negatively) charged monopoles. Charges are denoted inside the sphere. The insets (a), (b), and (c) show the degenerate states at  $R_5 = g, 0,$ , and  $-g$ , respectively; here  $R_1 = R_2 = R_3 = R_4 = 0$ . The inset (d) shows the effective Hamiltonian in the vicinity of  $R_5 = g, R_1 = R_2 = R_3 = R_4 = 0$ . Orange solid lines and black dots represent single particle states and bosons, respectively. Purple dotted arrows show effective couplings.

Other terms can be written similarly. Comparing with the expression in the main text, we have

$$c_N = \frac{\prod_{i=0}^{N-1} \sqrt{(N-i)(i+1)}}{\prod_{i=1}^{N-1} [(N-i)^2 + i^2 - N^2]}. \quad (\text{S40})$$

### TOPOLOGICAL INVARIANTS

The Wilson line  $W_{ij}(\phi)$  is defined by  $W_{ij}(\phi) = \langle \Psi_i(\pi, \phi) | \hat{W} | \Psi_j(0, \phi) \rangle$ , where  $|\Psi_{i=1,2}(0, \phi)\rangle$  and  $|\Psi_{i=1,2}(\pi, \phi)\rangle$  are the lowest two eigenstate states at the north and south poles, respectively,  $\phi \in [0, 2\pi)$  is the azimuthal angle, and  $\hat{W} = \prod_{k=1}^N \hat{P}_k$ ,  $\hat{P}_k = \sum_{i=1}^2 |\Psi_i(\theta_k, \phi)\rangle \langle \Psi_i(\theta_k, \phi)|$  is the projection operator in the  $k$ th step if we divide the longitude to  $N$  steps. Physically,  $W_{ij}(\phi)$  characterizes the probability of occupying either eigenstate at the south pole if the initial state is an arbitrary superposition of the eigenstate at the north pole after an adiabatic evolution along the longitude.  $W_{ij}(\phi)$  is an orthogonal matrix and can be made real after an appropriate unitary transformation on  $\hat{H}_{\text{eff}}$  (rotate  $\hat{H}_{\text{eff}}$  to be real). Thus,  $\xi(\phi) = W_{11}(\pi/2, \phi) + iW_{12}(\pi/2, \phi)$  defines a winding number  $n_w = -\frac{i}{2\pi} \int_0^{2\pi} \xi^*(\phi) \partial_\phi \xi(\phi)$ .

### 3D TOPOLOGICAL DEFECTS FOR EVEN NUMBER OF PARTICLES WITH REPULSIVE INTERACTION

For later convenience, we introduce  $R_A$ ,  $R_B$ ,  $\phi_A$ , and  $\phi_B$ , which are defined through  $R_A e^{-i\phi_A} = R_x - iR_y$  and  $R_B e^{-i\phi_B} = R_z n_x - iR_z n_y$ . For  $4m$  particles with strong repulsive interaction, the ground state is  $|m, m, m, m\rangle$ . No degeneracy is found.

For  $4m + 2$  particles with strong repulsive interaction, the ground state manifold has 6 states,  $|m, m, m+1, m+1\rangle, |m, m+1, m, m+1\rangle, |m, m+1, m+1, m\rangle, |m+1, m, m, m+1\rangle, |m+1, m, m+1, m\rangle$ , and  $|m+1, m+1, m, m\rangle$ . The Hamiltonian reads

$$\begin{pmatrix} 0 & 0 & -e^{i\phi_B}(m+1)R_B & -e^{i\phi_B}(m+1)R_B & 0 & 0 \\ 0 & 0 & e^{i\phi_A}(m+1)R_A & -e^{i\phi_A}(m+1)R_A & 0 & 0 \\ -e^{-i\phi_B}(m+1)R_B & e^{-i\phi_A}(m+1)R_A & 2R_5 & 0 & -e^{i\phi_A}(m+1)R_A & -e^{i\phi_B}(m+1)R_B \\ -e^{-i\phi_B}(m+1)R_B & -e^{-i\phi_A}(m+1)R_A & 0 & -2R_5 & e^{i\phi_A}(m+1)R_A & -e^{i\phi_B}(m+1)R_B \\ 0 & 0 & -e^{-i\phi_A}(m+1)R_A & e^{-i\phi_A}(m+1)R_A & 0 & 0 \\ 0 & 0 & -e^{-i\phi_B}(m+1)R_B & -e^{-i\phi_B}(m+1)R_B & 0 & 0 \end{pmatrix} \quad (\text{S41})$$

Two of the states, i.e.  $(|0, 0, 1, 1\rangle - e^{-2i\phi_B} |1, 1, 0, 0\rangle)/\sqrt{2}$  and  $(|0, 1, 0, 1\rangle + e^{-2i\phi_A} |1, 0, 1, 0\rangle)/\sqrt{2}$ , have zero energy.

Projecting out these two states, we write the effective Hamiltonian as a 4 by 4 matrix,

$$\begin{pmatrix} 2R_5 & \sqrt{2}e^{-i\phi_A}(m+1)R_A & -\sqrt{2}e^{-i\phi_B}(m+1)R_B & 0 \\ \sqrt{2}e^{i\phi_A}(m+1)R_A & 0 & 0 & -\sqrt{2}e^{i\phi_A}(m+1)R_A \\ -\sqrt{2}e^{i\phi_B}(m+1)R_B & 0 & 0 & -\sqrt{2}e^{i\phi_B}(m+1)R_B \\ 0 & -\sqrt{2}e^{-i\phi_A}(m+1)R_A & -\sqrt{2}e^{-i\phi_B}(m+1)R_B & -2R_5 \end{pmatrix}. \quad (\text{S42})$$

Rewriting the effective Hamiltonian using direct product of  $\sigma$  and  $\tau$  matrices, we obtain

$$R_5(\tau_z + \sigma_z) + (R'_1\sigma_x + R'_2\sigma_y - R'_3\tau_x + R'_4\tau_y + \tau_z(R'_3\tau_x + R'_4\tau_y) + \tau_z(R'_1\tau_x - R'_2\tau_y)), \quad (\text{S43})$$

where  $R'_1 = (m+1)(R_1 - R_3)/\sqrt{2}$ ,  $R'_2 = (m+1)(R_2 + R_4)/\sqrt{2}$  and  $R'_3 = (m+1)(R_1 + R_3)/\sqrt{2}$ , and  $R'_4 = (m+1)(R_2 - R_4)/\sqrt{2}$ . Solving the effective Hamiltonian, the eigen energies reads

$$\pm \sqrt{2}(m+1) \sqrt{\pm \sqrt{\left( (R_A^2 + R_B^2) + \frac{R_5^2}{(m+1)^2} \right)^2 - 4R_A^2 R_B^2 + R_A^2 + R_B^2 + \frac{R_5^2}{(m+1)^2}}}. \quad (\text{S44})$$

Eigenenergies become degenerate in certain 3D continuous manifolds.

$\{\mathcal{M}_1: R_A = 0\}$  and  $\{\mathcal{M}'_1: R_B = 0\}$ , the second and the third states are degenerate, and the ground state (the fourth state) is unique.

$\{\mathcal{M}_2: R_5 = 0, R_A = R_B\}$ , both the ground and excited states are doubly degenerate.

For  $M_1$  and  $M'_1$ , we find that the berry phase  $\gamma = (0, 2\pi, 2\pi, 0)$  and  $\zeta_1 = 0$  for the lowest two states. For  $M_2$ , we find that  $\gamma = \pi$  for all eigenstates and  $\zeta_1 = 0$  for the lowest two states.

We also rewrite the manifolds in the main text using  $R_A$  and  $R_B$  and find that the two type of 3D manifolds are switched with each other as the interaction strength changes from negative to positive. Furthermore, we have numerically verified that these degenerate manifolds extend to the weakly interacting regime.

## LINKING NUMBER

In the 3D subspace with finite  $|\vec{m}|$ , e.g.,  $R_3 \neq 0$  and  $R_4 = 0$ ,  $\mathcal{M}_1$  and  $\mathcal{M}_2$  are knotted nodal line and nodal ring. Thus, a linking number can be defined as follows,

$$L = \frac{1}{4\pi} \oint_{\mathcal{M}_1} \oint_{\mathcal{M}_2} \frac{\mathbf{r}_1 - \mathbf{r}_2}{|\mathbf{r}_1 - \mathbf{r}_2|^{\frac{3}{2}}} \cdot d\mathbf{r}_1 \times d\mathbf{r}_2. \quad (\text{S45})$$

A straightforward calculation shows that  $L$  is always 1, which verifies that the two nodal surfaces are knotted in the subspace.

## EXPERIMENTAL SCHEMES FOR EXPLORING FEW-BODY PHYSICS

There are a number of schemes to experimentally explore few-body physics related to the discussions in the main text, including optical superlattice, mesoscopic traps, optical tweezers, ion traps, and superconducting circuits.

As shown in Fig. S4(A), a 2D optical superlattice is formed by a short and long lattice with wavelengths  $\lambda_L = 2\lambda_S$  [32, 34]. Such superlattice divides the system into many plaquettes. When the energy barrier between different plaquettes is large enough, plaquettes are isolated from each other. Each contains a few particles, and can be dressed and probed individually. In particular, high resolution in-situ images allow experimentalists to measure precisely the particle number per plaquette. Optical superlattices have allowed physicists to explore many interesting few-body phenomena in two sites or four sites.

To induce complex tunnelings among the four sites, either Raman dressing or shaking can be used. In the former approach, a field gradient can be applied in the diagonal direction to quench the bare tunnelings along both  $x$  and  $y$  directions [32, 34]. Then a pair of Raman laser induces a complex laser assisted tunneling. In fact, it is not necessary to individually control the phase of each tunneling. The key requirement is that the total effective magnetic flux per plaquette is  $\pi$ , i.e., a particle accumulates a  $\pi$  phase after finishing a closed loop composed of all four sites. Another approach is shaking the lattice [41, 42]. Theoretically, this is the same as the Raman dressed lattice. In practice, the advantage is that, no extra lasers are required. The onsite energies can be tuned by the two-photon detuning or the

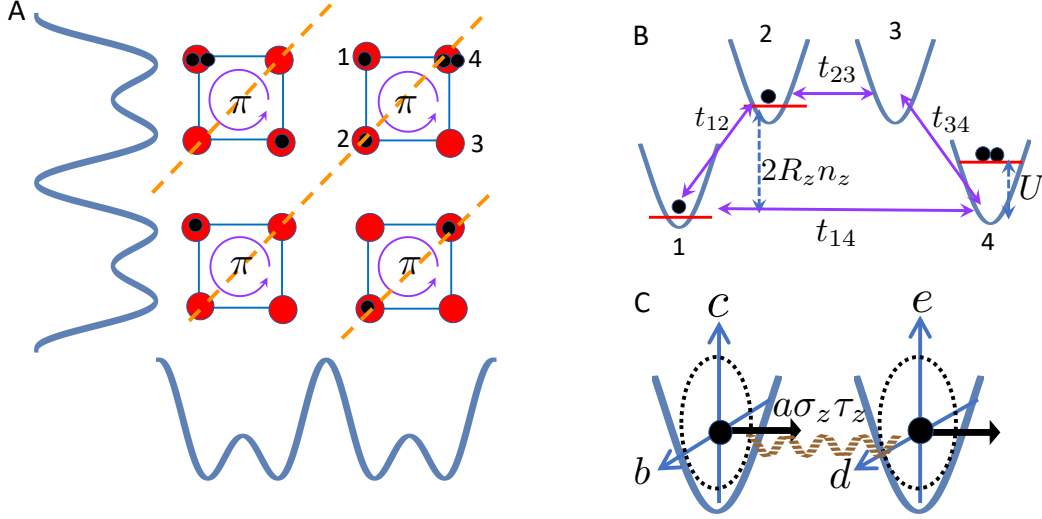


FIG. S4. (Color online) (A) Red spheres represent lattice sites of an optical superlattice and blue curves represent lattice potentials. Black spheres represent atoms. Orange dashed lines represent an additional lattice potential that shifts the onsite energies of two sites in each plaquette. (B) A schematic of the tunnelings and onsite energy in four mesoscopic traps, optical tweezers, or each plaquette of an optical superlattice. (C) Our results also apply to two ion traps, each of which hosts a spin-1/2 (black arrows).

shaking frequency. An additional 1D optical lattice aligned in the diagonal direction can provide extra controls of the onsite energy. Using typical experimental parameters for Rb with scattering length  $\approx 5\text{nm}$  and laser wavelength  $767\text{nm}$ , we find that, interaction strength  $g$  in such lattice can reach  $100\text{Hz}$ . For other atoms, Feshbach resonance could further enhance  $g$ .  $g$  is the characteristic energy scale of topological defects discussed here, for instance, the separation between different Yang monopoles in the parameter space and the energy gap in the effective models. With such  $g$ , topological defects can be easily resolved in current experiments.

One could also use four mesoscopic traps [27, 28], or optical tweezers to realize a four-site system that is equivalent to a single plaquette, as shown in Fig. S4(B). Two optical tweezers have been recently used to produce entangled pairs of atoms [43]. For instance, bringing four tweezers together and engineering the tunnelings between tweezers using external lasers, a single four-site model could be realized. Alternatively, one could stick to a single tweezer, and use four internal states of atoms. Theoretically, this would be equivalent to the NIST experiment. The advantage here is that, due to the strong confinement in an optical tweezer, the interactions could be much stronger. For instance, the typical confining potential of a single optical tweezer is  $200\text{kHz}$ . For Rb with scattering length  $a_s = 5\text{nm}$  and Cs with scattering length  $a_s = 91\text{nm}$ , such confinement corresponds to an interaction strength  $1\text{kHz}$  and  $24\text{kHz}$ , respectively. Thus, it will be much easier to explore interaction induced topological defects in optical tweezers.

Other quantum systems other than cold atoms can also be used to explore topological defects discussed in the main text. For instance, two nearby ion trap, each of which hosts a spin-1/2, can be used to realize the model in Eq.(7) of the main text, as shown in Fig. (S2.C). Here,  $(b, c)$  and  $(d, e)$  represent the magnetic field acting on the first and the second spin-1/2, which is denoted by  $\vec{\sigma}$  and  $\vec{\tau}$ , respectively, in the  $x - y$  plane.  $a\sigma_z\tau_z$  is simply the Ising interaction. Similarly, two superconducting circuits may be used, as each circuit can be viewed as a spin-1/2 [44, 45]. Therefore, our theoretical results can also be generalized to superconducting circuits.

## GENERIC INTERACTION

A generic interaction  $\sum_i g_i n_i^2 + \sum_{i \neq j} g_{ij} n_i n_j$  leads to corrections to the effective Hamiltonian discussed in the main text. As interactions transform to the onsite energy in the effective Hamiltonians constructed by four Fock states in Eq. (1) and Eq. (7) of the main text, nonuniform  $g_i$  and nonlocal  $g_{i \neq j}$  (or equivalently, the inter-spin interaction in the spin model) only lead to corrections in the diagonal terms. Most generically, the corrections can be written as

$\hat{H}'_{eff} = \sum_i \delta_i H'_i$ , where

$$\begin{aligned} H'_1 &= \sum_{i=1}^4 \hat{a}_i^\dagger \hat{a}_i, \\ H'_2 &= \hat{a}_1^\dagger \hat{a}_1 + \hat{a}_2^\dagger \hat{a}_2 - \hat{a}_3^\dagger \hat{a}_3 - \hat{a}_4^\dagger \hat{a}_4, \\ H'_3 &= \hat{a}_1^\dagger \hat{a}_1 - \hat{a}_2^\dagger \hat{a}_2 - \hat{a}_3^\dagger \hat{a}_3 + \hat{a}_4^\dagger \hat{a}_4, \\ H'_4 &= \hat{a}_1^\dagger \hat{a}_1 - \hat{a}_2^\dagger \hat{a}_2 + \hat{a}_3^\dagger \hat{a}_3 - \hat{a}_4^\dagger \hat{a}_4. \end{aligned} \quad (\text{S46})$$

and  $\delta_i$  corresponds to the strength of each type of perturbation.

$\delta_i$  depend on  $g_i$  and  $g_{ij}$ . For instance, the effective Hamiltonian near the origin of the parameter space for odd number of particles reads

$$\begin{pmatrix} -c_1 R_5 + \delta_1 + \delta_2 + \delta_3 + \delta_4 & -c_2 (R_1 - iR_2) & -c_2 (R_3 - iR_4) & 0 \\ -c_2 (R_1 - iR_2) & c_1 R_5 + \delta_1 + \delta_2 - \delta_3 - \delta_4 & 0 & -c_2 (R_3 - iR_4) \\ -c_2 (R_3 - iR_4) & 0 & c_1 R_5 + \delta_1 - \delta_2 - \delta_3 + \delta_4 & c_2 (R_1 - iR_2) \\ 0 & -c_2 (R_3 - iR_4) & c_2 (R_1 - iR_2) & -c_1 R_5 + \delta_1 - \delta_2 + \delta_3 - \delta_4 \end{pmatrix} \quad (\text{S47})$$

where  $c_1 = \tilde{\epsilon}_i/\epsilon_i$  and  $c_2 = \tilde{t}_{ij}/t_{ij}$  [rewrite of Eq. (5) in the main text]. For three particles,  $c_1 = -1$ ,  $c_2 = 1$ , and

$$\delta_1 = \frac{1}{4} (3g_1 + 3g_2 + 3g_3 + 3g_4 + 2g_{12} + 2g_{13} + 2g_{14} + 2g_{23} + 2g_{24} + 2g_{34}) \quad (\text{S48})$$

$$\delta_2 = \frac{1}{4} (-g_1 - g_2 + g_3 + g_4 - 2g_{12} + 2g_{34}) \quad (\text{S49})$$

$$\delta_3 = \frac{1}{4} (-g_1 + g_2 + g_3 - g_4 - 2g_{14} + 2g_{23}) \quad (\text{S50})$$

$$\delta_4 = \frac{1}{4} (-g_1 + g_2 - g_3 + g_4 - 2g_{13} + 2g_{24}). \quad (\text{S51})$$

For systems with equal intraspin interaction and no interspin interaction, i.e.,  $g_i = g$ , and  $g_{ij} = 0$ , we obtain  $\delta_1 = 3g$  and  $\delta_2 = \delta_3 = \delta_4 = 0$ . The Hamiltonian reduces to the unperturbed one.

For generic cases where  $\delta_i \neq 0$ , these four corrections  $H'_i$  can be classified into two categories.

Category 1:  $H'_1$  and  $H'_3$  respect time reversal symmetry of the effective Hamiltonian.  $H'_1$  only shifts the entire energy spectrum and does not change the topological defects.  $H'_3$  only shifts the position of the topological defects as a finite  $\delta_3$  simply changes the value of  $R_5$  to  $R_5 - \delta_3$ . Therefore, the shape of topological defects and other results in the main text remain unchanged.

Category 2:  $H'_2$  and  $H'_4$  break the time reversal symmetry and new topological defects arise.

When only  $H'_2$  exists, i.e.,  $\delta_2 \neq 0, \delta_4 = 0$ , the energy spectrum reads

$$E_{eff} = \pm \sqrt{\pm 2\sqrt{\delta_2^2 (R_1^2 + R_2^2 + R_5^2)} + R_1^2 + R_2^2 + R_3^2 + R_4^2 + \delta_2^2 + R_5^2}. \quad (\text{S52})$$

The two degenerate manifolds are obtained as follows.

1.  $\mathcal{M}_1$ , the first (third) and the second (fourth) states become degenerate when  $R_5 = R_1 = R_2 = 0$ .

2.  $\mathcal{M}_2$ , the second and the third states become degenerate when  $R_5^2 + R_1^2 + R_2^2 = \delta_2^2$  and  $R_3 = R_4 = 0$ .

Apparently,  $\mathcal{M}_1$  is an infinite 2D topological defect. In contrast,  $\mathcal{M}_2$  becomes a finite 2D sphere, unlike  $\mathcal{M}_2$  discussed in the main text, which extends to infinity. Thus, a finite  $\delta_2$  breaks the four-fold degeneracy at the original Yang monopole but retains the degeneracy between the second and the third states on a 2D sphere,  $\mathcal{M}_2$ .

Likewise, when only  $H'_4$  exists, i.e.,  $\delta_4 \neq 0, \delta_2 = 0$ , we also obtain two degenerate manifolds,

1.  $\mathcal{M}_1$ , the first (third) and the second (fourth) state become degenerate when  $R_5 = R_3 = R_4 = 0$ .

2.  $\mathcal{M}_2$ , the second and the third states become degenerate when  $R_5^2 + R_3^2 + R_4^2 = \delta_4^2$  and  $R_1 = R_2 = 0$ .

Again,  $\mathcal{M}_1$  is an infinite 2D topological defect, and  $\mathcal{M}_2$  is a finite 2D sphere.

When both  $H'_2$  and  $H'_4$  exist, i.e.,  $\delta_2 \neq 0$  and  $\delta_4 \neq 0$ ,  $\mathcal{M}_2$  can be written as,

$$\frac{R_5^2}{\delta_4^2} + \frac{R_3^2 + R_4^2}{(\delta_4^2 - \delta_2^2)} = 1, \quad |\delta_2| < |\delta_4| \quad (\text{S53})$$

$$\frac{R_5^2}{\delta_2^2} + \frac{R_1^2 + R_2^2}{(\delta_2^2 - \delta_4^2)} = 1, \quad |\delta_2| > |\delta_4| \quad (\text{S54})$$

For generic  $\delta_2 \neq 0$  and  $\delta_4 \neq 0$ , Eqs. (S53) and (S54) describe an ellipsoid. It is clear that, when  $\delta_2 = 0$  or  $\delta_4 = 0$ , Eqs. (S53) and (S54) reduce to the previous results. When  $|\delta_2| = |\delta_4|$ ,  $\mathcal{M}_2$  becomes a line segment connecting  $(0, 0, 0, 0, -\delta_2)$  and  $(0, 0, 0, 0, \delta_2)$ , which signifies the transition from one ellipsoid in Eq.(S53) to the other in Eq.(S54).

In any case, if a 4D sphere encloses  $\mathcal{M}_2$ ,  $C_2$  remains unchanged. The reason is that, the second Chern number, as a topological invariant, is stable against small perturbations. Unless the perturbation is strong enough to close the energy gap between the second and the third energy eigenstates,  $C_2$  remains the same. Thus, when the amplitudes of perturbations are much smaller than parameters of the single-particle Hamiltonian, for instance, the distance to the origin of the five-dimensional parameter space,  $R$ , results of  $C_2$  in the main text remain unchanged.

We have also generalized the above results to the effective Hamiltonian for 3D continuous topological defects, i.e., the effective Hamiltonian in Eq.(7) of the main text. For two particles, if either  $\delta_2$  and  $\delta_4$  is zero,  $\mathcal{M}_1$  is defined as  $R_1 = R_2 = R_5 = 0$ . If both  $\delta_2$  and  $\delta_4$  are finite,  $\mathcal{M}_1$  does not exist. In contrast,  $\mathcal{M}_2$  always exists. For finite  $\delta_2$  and  $\delta_4$ ,  $\mathcal{M}_2$  is shifted to  $R_5 = 0$  and  $R_1^2 + R_2^2 + \delta_4^2 = R_3^2 + R_4^2 + \delta_2^2$ . Thus, small nonuniform  $g_i$  and nonlocal interactions  $g_{i \neq j}$  only lead to perturbative changes to the topological defects.